

Homogeneous sensitivity of sol–gel derived planar waveguide structures – theoretical analysis

CUMA TYSZKIEWICZ

Department of Optoelectronics, Silesian University of Technology,
ul. Bolesława Krzywoustego 2, 44-100 Gliwice, Poland;
e-mail: cuma.tyszkiewicz@polsl.pl

Rib waveguides are the key components of integrated optical devices including evanescent wave chemical and biochemical sensors. The sol–gel method allows the $\text{SiO}_2\text{:TiO}_2$ rib waveguides with very low attenuation to be fabricated by means of selective etching of the $\text{SiO}_2\text{:TiO}_2$ parent slab waveguides deposited on glassy substrates. The present work focuses on theoretical investigation into both the influence of selected rib waveguide geometrical parameters and wavelength on the homogeneous sensitivity of the rib waveguides. The homogeneous sensitivity spectral characteristics of rib waveguides are compared with the ones for the parent slab waveguides. Moreover, there is investigated the influence of additional, sol–gel based amorphous silica layer, which separates rib sidewalls from an ambient on effective index and homogeneous sensitivity characteristics. Analysis was carried out using effective index method.

Keywords: rib waveguides, optical sensors.

1. Introduction

An important goal of research into the integrated optics is the development of low-loss waveguides compatible with existing silicon based technologies to allow integration with electrical devices and lab-on-chip designs [1–3]. Waveguides in use can be either homostructural or heterostructural. Waveguides fabricated by means of ion exchange in glass [4], Ti diffusion into LiNbO_3 substrates [5] or obtained by admixture of semiconductor materials (GaAs, InP) [6, 7] are homostructural. Homostructural waveguides are characterized by gradient profiles and low refractive index contrasts. In turn, the production process of heterostructural waveguides consists of two steps. In the first step, a uniform slab waveguide is produced. In the second step, this slab is selectively etched making a rib channel waveguide. The relatively chip and robust method, compared to PECVD (plasma enhanced chemical vapour deposition), LPCVD (low pressure chemical vapour deposition) and MOCVD (metal organic chemical vapour deposition), which allows fabrication of extremely low-loss $\text{SiO}_2\text{:TiO}_2$ rib waveguides is based on the combination of sol–gel technology and chemical etching. Such waveguides were previously fabricated and characterized by KARASIŃSKI *et al.* [8–12].

The sol–gel technology allows easier fabrication [13–15] and optimization [16] of sensor structures utilizing evanescent wave spectroscopy, and for that reason it is used in optical sensors and biosensors with application in environmental monitoring and medicine [17]. When a slab or a rib waveguide is used in a planar evanescent wave chemical or biochemical sensor (PEWS) the physical effects behind the operating principle of the sensor may rely on a change of effective indexes of guided modes [18, 19]. If the assumption is taken that a refractive index of the homogeneous and semi-infinite cover layer is changed, then the relationship between this and the effective refractive index is given by the equation:

$$\Delta n_{\text{eff}} = S_H \Delta n_c \quad (1)$$

where $S_H = dn_{\text{eff}}/dn_c$ is the homogeneous sensitivity.

This paper is devoted to theoretical analysis of a relation between the selected geometrical parameters of $\text{SiO}_2:\text{TiO}_2$ rib waveguides and their homogeneous sensitivity. The sensitivity characteristics of the rib waveguides are compared with corresponding characteristics of the parent slab waveguides. The smallest detectable changes in the cover refractive index $(\Delta n_c)_{\text{min}}$ are calculated under the assumption that phase detection uses the differential interference between the $\text{TE}_0\text{--TM}_0$ modes in the case of the slab waveguides and between the $\text{TE}_{00}\text{--TM}_{00}$ modes in rib waveguides. Moreover, the sidewall imperfections of rib waveguides behave as sources of attenuation, which in turn is directly proportional to the squared difference of both rib waveguide refractive index and cover refractive index squares [20]. Therefore, there is evaluated the influence of the additional silica layer, separating the rib sidewalls from the ambient, on the sensitivity characteristics and detection limit $(\Delta n_c)_{\text{min}}$.

2. Waveguide structures

The investigated planar structure is composed of an $\text{SiO}_2:\text{TiO}_2$ waveguide film deposited on a BK7 glass substrate. Detailed information about fabrication technology is given in Ref. [8]. The morphological parameters of the rib waveguide structures investigated as well as of the parent slab waveguide are schematically presented in Figure 1.

The parent slab waveguide is characterized by the thickness H , and by the refractive indexes of the $\text{SiO}_2:\text{TiO}_2$ waveguide film n_r , BK7 substrate n_s and cover refractive index n_c , respectively. Besides, the rib waveguides are characterized by two or four additional parameters: height t , width w , refractive index n_{cs} and thickness h_{cs} of the amorphous silica film separating the sidewalls of the rib from the cover (ambient).

The complex refractive indexes $\tilde{n} = n + i\kappa$ of respectively the $\text{SiO}_2:\text{TiO}_2$ films and silica films have been determined by the ellipsometric method using a spectroscopic ellipsometer Woollam M-2000. These studies were carried out in the wavelength range from 190 nm up to 1700 nm. The measurements were performed for the angles of incidence of 60°, 65° and 70°. During the measurements, the relative humidity in the room was about 52%, and the temperature was 20 °C. In the case of $\text{SiO}_2:\text{TiO}_2$

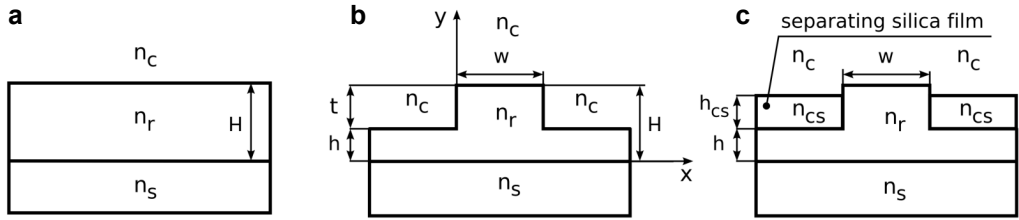


Fig. 1. Diagram of the parent slab and the rib waveguides: (a) parent slab, (b) rib with unmasked sidewalls, (c) rib with sidewalls separated from an ambient with a silica layer. Description of parameters: n_r , n_s , n_c , n_{cs} – refractive indexes of SiO₂:TiO₂ waveguide film, BK7 substrate, cover (ambient), separating silica film, H – parent slab thickness, t – rib height, w – rib width, h – thickness of etched slab, h_{cs} – thickness of separating silica film.

films the spectral dependencies of ellipsometer angles ψ and Δ were fitted with extended Cauchy formula. The chromatic dispersion of the refractive index real part is given by the equation:

$$n(\lambda) = A + \frac{B}{\lambda^2} + \frac{C}{\lambda^4} \tag{2}$$

where: $A = 1.751$, $B = 6.077 \times 10^{-3}$, $C = 2.751 \times 10^{-3}$.

For silica films the chromatic dispersion of the refractive index real part is given by the Sellmeier equation:

$$n^2(\lambda) = 1 + \sum_{j=1}^3 \frac{A_j \lambda^2}{\lambda^2 - B_j} \tag{3}$$

where: $A_1 = 0.7$, $B_1 = 4.703 \times 10^{-3}$, $A_2 = 0.4$, $B_2 = 1.355 \times 10^{-2}$, $A_3 = 0.897$, $B_3 = 97.89$.

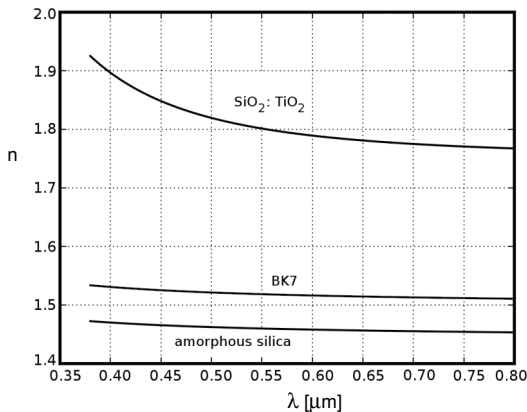


Fig. 2. Refractive index real part dispersion $n(\lambda)$ of the SiO₂:TiO₂ films, amorphous silica films and BK7 substrates.

The chromatic dispersion of BK7 glass refractive index is also given by the Sellmeier equation. The detailed information of Sellmeier coefficients of BK7 were culled from a datasheet published by SCHOOT AG. The analysis presented in this paper is limited to the wavelength range from 380 nm to 800 nm. In this range the extinction coefficient κ can be neglected for all these three materials. The chromatic dispersions of the materials under study are shown in Fig. 2, with the measurement uncertainty of the refractive index real part less than 0.001.

3. Effective index method formulation

The analysis of rib waveguides was carried out with the application of the effective-index method (EIM) [21]. The basic assumption of EIM method is that the electromagnetic field can be expressed with the separation of spatial variables. For the normalized electric field component $E(x, y)$, the solution to Helmholtz equation is given by:

$$E(x, y) = F_i(x)G_i(y) \tag{4}$$

where $i = x, y$ denotes the direction of polarization of the normalized electric field components: $F_i(x)$ and $G_i(y)$.

The diagram illustrating the application of EIM to the rib waveguide analysis is shown in Fig. 3. The above-mentioned separation narrows down the analysis of

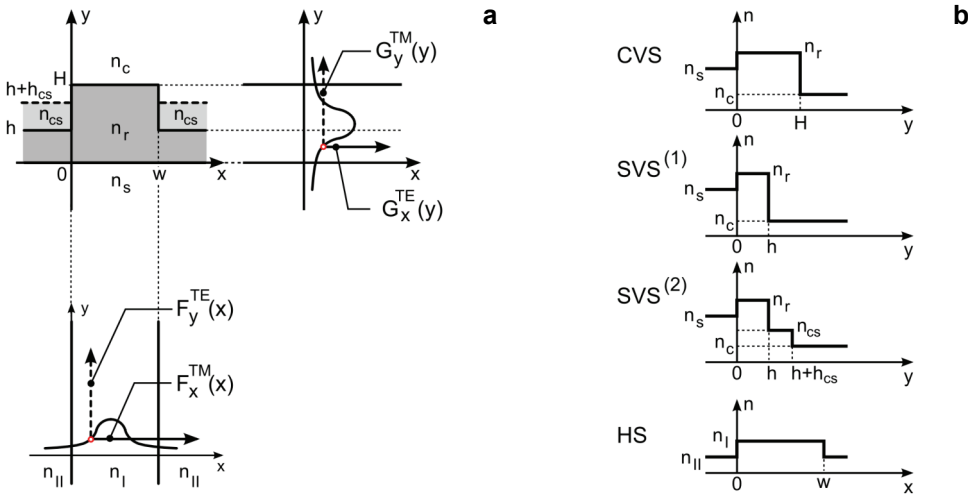


Fig. 3. Application of the effective index method to a rib waveguide. (a) The relationship between normalized electric field components $F(x)$, $G(y)$ and normalized electric field modal distributions of the CVS and HS slab waveguides. (b) Refractive index profiles of CVS, SVS and HS slab waveguides. CVS – central vertical slab, SVS⁽¹⁾, SVS⁽²⁾ – side vertical slab in the case of rib with unmasked (1) and masked (2) sidewalls, HS – horizontal slab. n_I , n_{II} , n_{III} – effective indexes of CVS, SVS and HS, respectively, $G_x^{TE}(y)$, $G_y^{TM}(y)$ – normalized principal electric field components of TE and TM modes of order q ($= 0, 1, 2, \dots$) of CVS, $F_x^{TE}(y)$, $F_x^{TM}(y)$ – normalized principal electric field components of TE and TM modes of order p ($= 0, 1, 2, \dots$) of the HS.

the rib waveguide to an analysis of three slab waveguides marked with the acronyms: CVS (central vertical slab), SVS (side vertical slab) and HS (horizontal slab). In the first step, the effective indexes n_I of the CVS: $[n_s:n_r, H:n_c]$ and n_{II} of the SVS are calculated. The description of the SVS in the case of the rib with unmasked sidewalls is $[n_s:n_r, h:n_c]$, whereas the rib with masked sidewalls is four-layered: $[n_s:n_r, h:n_{cs}, h_{cs}:n_c]$. Taking the effective indexes n_I and n_{II} the HS $[n_{II}:n_I, w:n_{II}]$ is formed. The EIM method is applicable if SVS supports a single mode. The effective index n_{III} of the HS approximates the effective index of the rib waveguide. The dispersion equation applied for CVS is:

$$k_0 H \sqrt{n_r^2 - n_I^2} = q\pi + \sum_{x=s,c} \tan^{-1} \left[\left(\frac{n_r}{n_x} \right)^{2\rho} \sqrt{\frac{n_I^2 - n_x^2}{n_r^2 - n_I^2}} \right] \quad (5)$$

where: n_r, n_s, n_c are refractive indexes of the $\text{SiO}_2:\text{TiO}_2$ layer, substrate and cover, $\rho=0$ for a TE polarization and $\rho=1$ for a TM polarization, n_I is the effective index of the CVS, q ($=0, 1, 2, \dots$) is the mode number, H is the CVS thickness and $k_0 = 2\pi/\lambda$ is the free space wave number.

The dispersion equation applied for SVS when the sidewalls of the ribs are in direct contact with ambient is given by the equation:

$$k_0 h \sqrt{n_r^2 - n_{II}^2} = q\pi + \sum_{x=s,c} \tan^{-1} \left[\left(\frac{n_r}{n_x} \right)^{2\rho} \sqrt{\frac{n_{II}^2 - n_x^2}{n_r^2 - n_{II}^2}} \right] \quad (6)$$

where n_{II} is the effective index of the SVS, and h is the SVS thickness, with the remaining symbols being the same as those in Eq. (5).

The dispersion equation applied for SVS when the sidewalls of the ribs are separated from an ambient and the condition $n_{II} > n_{cs}$ is fulfilled, is as follows:

$$k_0 (h + h_{cs}) \sqrt{n_r^2 - n_{II}^2} = q\pi + \tan^{-1} \left[\left(\frac{n_r}{n_s} \right)^{2\rho} \sqrt{\frac{n_{II}^2 - n_s^2}{n_r^2 - n_{II}^2}} \right] + \quad (7)$$

$$+ \tan^{-1} \left[\alpha \frac{\beta \cosh \gamma - \sinh \gamma}{\beta \cosh \gamma + \sinh \gamma} \right]$$

where:

$$\alpha = \left(\frac{n_r}{n_{cs}} \right)^{2\rho} \sqrt{\frac{n_{II}^2 - n_{cs}^2}{n_r^2 - n_{II}^2}}$$

$$\beta = \left(\frac{n_{cs}}{n_s} \right)^{2\rho} \sqrt{\frac{n_{II}^2 - n_c^2}{n_{II}^2 - n_{cs}^2}}$$

$$\gamma = k_0 h_{cs} \sqrt{n_{II}^2 - n_{cs}^2}$$

and n_{II} is the effective index of the SVS, h and h_{cs} are thicknesses of the $\text{SiO}_2:\text{TiO}_2$ and silica layers, respectively, and the remaining symbols denote the same as in Eq. (5).

Finally the dispersion equation for the HS is given by:

$$k_0 w \sqrt{n_I^2 - n_{II}^2} = p\pi + 2 \tan^{-1} \left[\left(\frac{n_I}{n_{II}} \right)^{2\rho} \sqrt{\frac{n_{III}^2 - n_{II}^2}{n_I^2 - n_{II}^2}} \right] \quad (8)$$

where n_{III} is the effective index of the HS, $p(= 0, 1, 2, \dots)$ is the mode number, w is the rib width, and the remaining symbols the same as those used in Eqs. (5) and (6).

The principal electric field component of a quasi- TE_{pq} mode of a rib waveguide is given by the equation:

$$E_{pq}^{\text{TE}}(x, y) = G_x^{\text{TE}}(y) F_x^{\text{TM}}(x) \quad (9)$$

The principal electric field component of a quasi- TM_{pq} mode of a rib waveguide is given by the equation:

$$E_{pq}^{\text{TM}}(x, y) = G_y^{\text{TM}}(y) F_y^{\text{TE}}(x) \quad (10)$$

4. Slab waveguides effective index and sensitivity characteristics

In this paragraph, the characteristics of the parent slab waveguide are presented. Its morphological parameters are referred to in Fig. 1a. We assume the thickness of the parent slab waveguide to be $H = 0.225 \mu\text{m}$. The spectral effective index

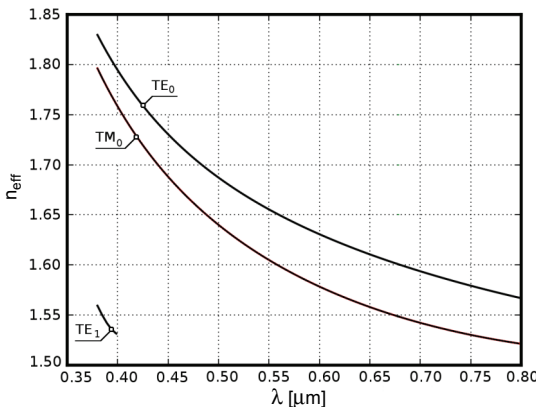


Fig. 4. Effective index spectral characteristics $n_{\text{eff}}(\lambda)$ of the parent slab waveguide, whose morphological parameters are presented in Fig. 1a. Characteristics calculated for $H = 0.225 \mu\text{m}$.

characteristic of the parent slab waveguide is shown in Fig. 4. For wavelengths greater than 0.4 μm it is single modal.

In Figure 5, the effective index (solid lines) and homogeneous sensitivity (dashed lines) characteristic of the parent slab waveguide as a function of its cover refractive index, for wavelength $\lambda = 0.677 \mu\text{m}$ are presented. It can be seen that homogeneous sensitivity is increasing with the increase in n_c due to the increase in a linear density of the optical power in the cover layer.

The homogeneous sensitivity is also wavelength dependent. Figure 6 shows the spectral characteristics of the homogeneous sensitivity. These characteristics allow us to estimate the smallest detectable change in a refractive index of the cover $(\Delta n_c)_{\min}$. Taking an assumption that changes in phase can be measured with 8-bit an accuracy

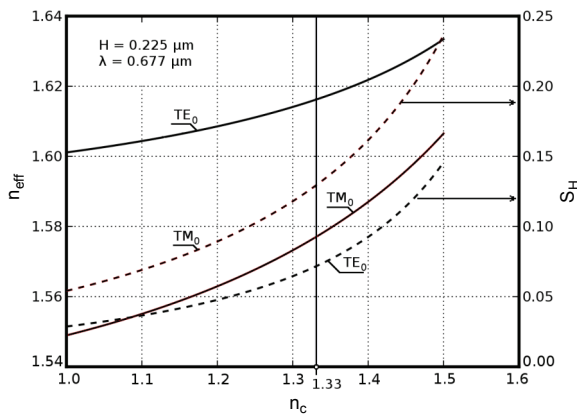


Fig. 5. Effective index n_{eff} and homogeneous sensitivity S_H characteristics of the parent slab waveguide as a function of a cover refractive index n_c . Morphological parameters of the parent slab are presented in Fig. 1a. Characteristics calculated for $H = 0.225 \mu\text{m}$ and $\lambda = 0.677 \mu\text{m}$.

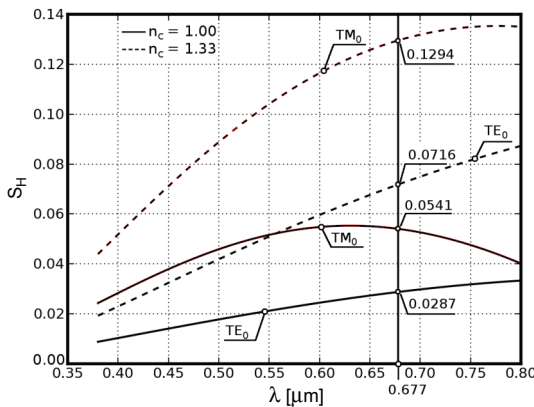


Fig. 6. Homogeneous sensitivity spectral characteristics $S_H(\lambda)$ of the parent slab waveguide calculated for the two values of the cover refractive index: $n_c = 1.00$ and $n_c = 1.33$. Morphological parameters of the parent slab are presented in Fig. 1a. Characteristics calculated for $H = 0.225 \mu\text{m}$.

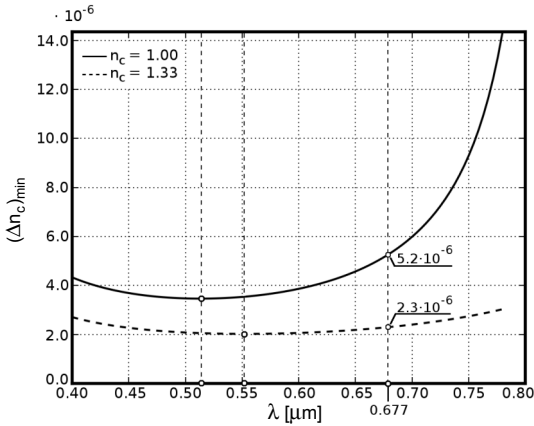


Fig. 7. Spectral characteristics of the cover refractive index detection limit $(\Delta n_c)_{\min}$ for a parent slab waveguide calculated for the two values of the cover refractive index: $n_c = 1.00$ and $n_c = 1.33$. The characteristics are calculated taking an assumption that there occurs the differential interference of TE_0 - TM_0 modes of the parent slab. Morphological parameters of the parent slab are presented in Fig. 1a. Characteristics calculated for $H = 0.225 \mu\text{m}$.

$\Delta\varphi_{\min} = \pi/256$, the path length is $L = 1 \text{ cm}$ and the differential interference of TM_0 - TE_0 modes is used, the minimal detection limit for $n_c = 1.00$ is $(\Delta n_c)_{\min} = 3.5 \times 10^{-6}$ at the wavelength $\lambda = 0.514 \mu\text{m}$, whereas for $n_c = 1.33$ it is $(\Delta n_c)_{\min} = 2.0 \times 10^{-6}$ at the wavelength $\lambda = 0.552 \mu\text{m}$.

The spectral characteristics of estimated detection limits are shown in Fig. 7. The wavelength at which the minimum of $(\Delta n_c)_{\min}$ is achieved is shifted towards shorter wavelengths comparing to the wavelength at which a difference between the effective indexes of orthogonal modes is maximal.

5. Rib waveguides

Additional parameters describing rib waveguides are: width w and height t . The former one is determined by a pattern on a photolithographic mask. In this paper, the assumption that $w = 2.0 \mu\text{m}$ was taken. The fabrication of the rib is carried out by means of a selective etching of the parent slab waveguide. Therefore, the effective index and homogeneous sensitivity characteristics of the rib waveguide as a function of thickness h of the etched part of the parent slab waveguide become relevant. The morphological parameters describing the rib waveguides are referred to in Fig. 1b and Fig. 1c.

5.1. Effective index characteristics

In Figure 8, the effective index characteristics of a rib waveguide are shown as a function of h calculated for wavelength $\lambda = 0.677 \mu\text{m}$. The rib waveguide is single modal for small etching depths $t < 12 \text{ nm}$. The EIM method is applicable for etching depths not exceeding $t^* = 45 \text{ nm}$.

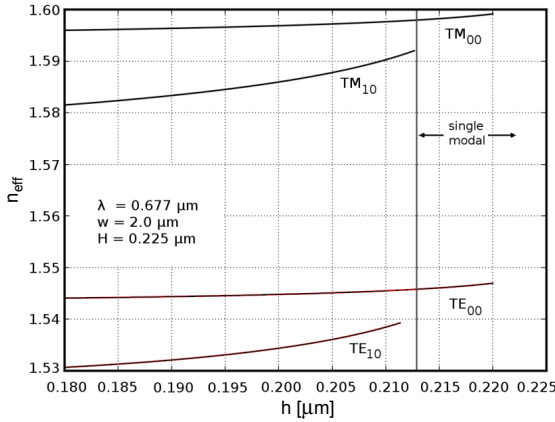


Fig. 8. The effective index n_{eff} characteristics of a rib waveguide as a function of thickness h of its parent slab waveguide. Morphological parameters of the rib are presented in Fig. 1b. Characteristics calculated for $H = 0.225 \mu\text{m}$, $w = 2.0 \mu\text{m}$, $n_c = 1.00$, $\lambda = 0.677 \mu\text{m}$.

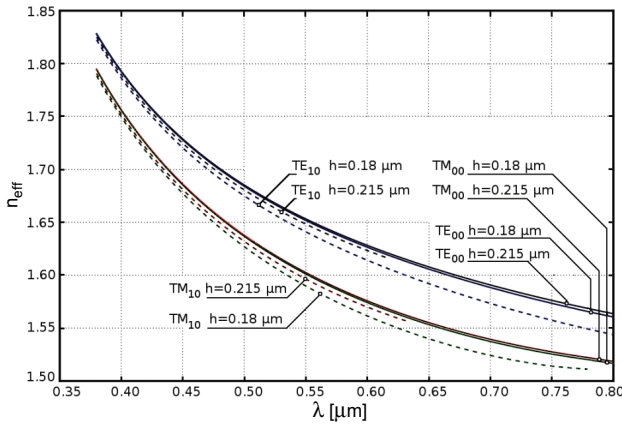


Fig. 9. The effective index spectral characteristics $n_{\text{eff}}(\lambda)$ of rib waveguides for two values of etching depth. Morphological parameters of these waveguides are presented in Fig. 1b. Characteristics calculated for $H = 0.225 \mu\text{m}$, $w = 2.0 \mu\text{m}$, $n_c = 1.00$.

The spectral effective index characteristic of rib waveguides is presented in Fig. 9 and was calculated for two values of etching depth: $t = 10 \text{ nm}$ and 45 nm . The first corresponds to a shallow etched rib of $h = 0.215 \mu\text{m}$, whereas the second corresponds to a rib of $h = 0.18 \mu\text{m}$ where the EIM method meets its limitation. The increase in etching depth shifts the cut-off wavelength of TE_{10} and TM_{10} modes towards longer wavelengths.

5.2. Homogeneous sensitivity characteristics

Figure 10 shows the spectral characteristics of the homogeneous sensitivity $S_H(\lambda)$ of rib waveguides (solid lines) compared with the ones calculated for the parent slab

waveguide (dashed lines). They have a single local maximum λ_{sm} which is dependent on the polarization and cover refractive index. The maxima of $S_H(\lambda)$ for TE_0 and TE_{00} modes are present for the wavelengths longer than the right limit of the spectral range presented in Fig. 10. For the parent slab waveguide these values are: $\lambda_{sm} = 0.91 \mu\text{m}$ for $n_c = 1.00$ and $\lambda_{sm} = 1.10 \mu\text{m}$ for $n_c = 1.33$. For the rib waveguides these are: $\lambda_{sm} = 0.89 \mu\text{m}$ for $n_c = 1.00$ and $\lambda_{sm} = 1.07 \mu\text{m}$ for $n_c = 1.33$.

For each pair of the parent slab–rib characteristics, for the given polarization and cover refractive index, a wavelength exists for which the values of homogeneous sensitivities are equal. For shorter wavelengths the sensitivity of the rib waveguide is higher than that of the parent slab waveguide, whereas for longer wavelengths it is lower.

Under the same conditions as for the parent slab waveguide, the spectral characteristics of estimated detection limits of Δn_c were calculated for the rib

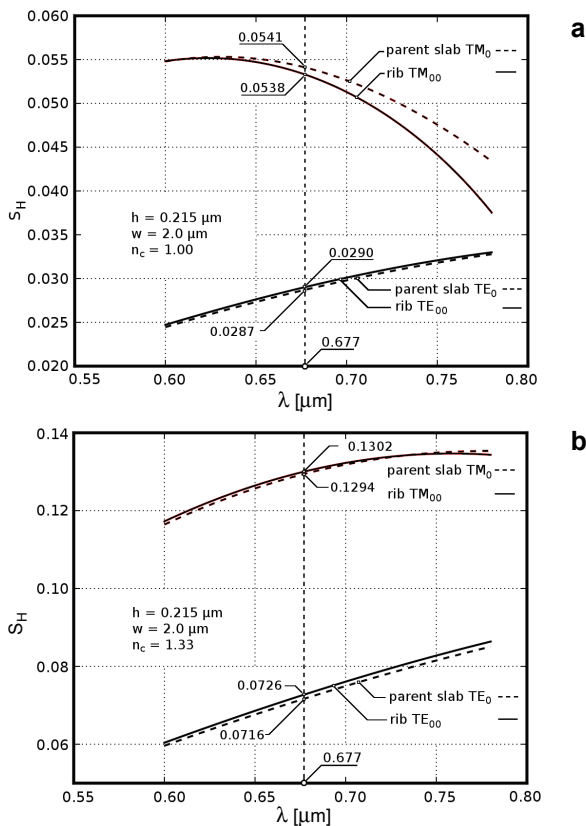


Fig. 10. Comparison of the homogeneous sensitivity spectral characteristics $S_H(\lambda)$ of parent slab waveguides and rib waveguides. Morphological parameters of these waveguides are presented in Figs. 1a and 1b. Characteristics calculated for $H = 0.225 \mu\text{m}$, $h = 0.215 \mu\text{m}$, $w = 2.0 \mu\text{m}$ and for the two values of the cover refractive index: $n_c = 1.00$ (a) and $n_c = 1.33$ (b).

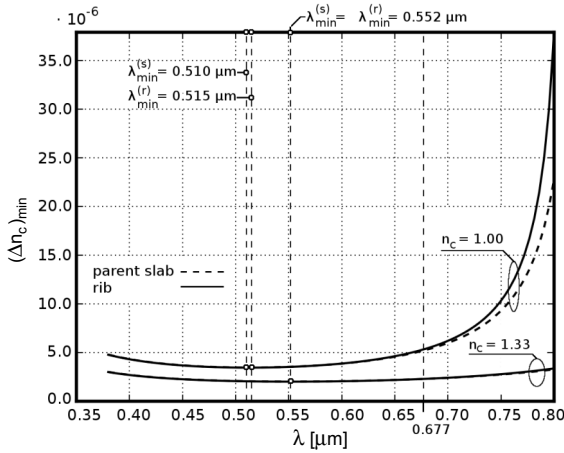
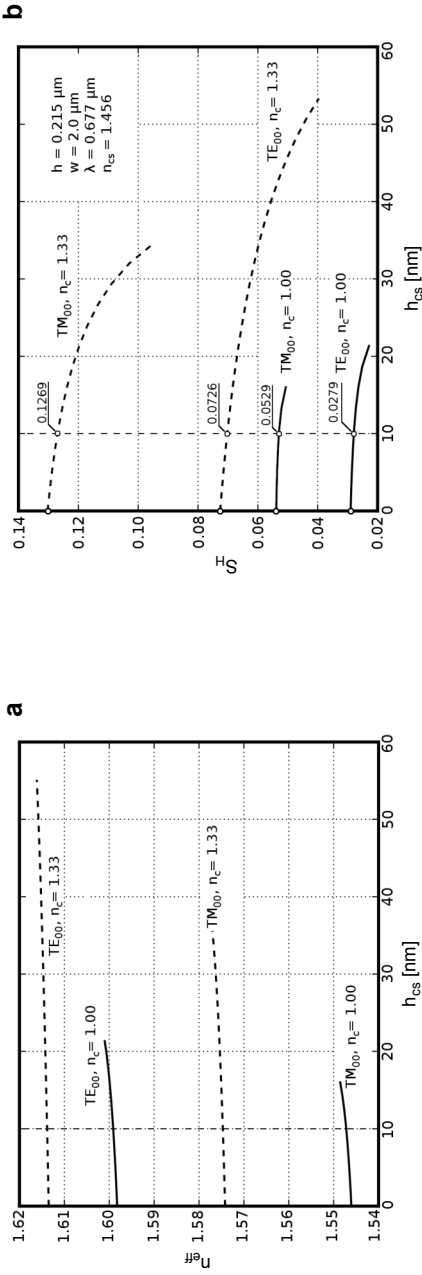


Fig. 11. The cover refractive index detection limit $(\Delta n_c)_{\min}$ spectral characteristics for the parent slab and the rib waveguide. The characteristics are calculated taking an assumption that there occurs the differential interference of TE_0 - TM_0 modes of the parent slab waveguide and TE_{00} - TM_{00} of the rib waveguide. Morphological parameters of the parent slab and rib waveguide are presented in Figs. 1a and 1b. Characteristics calculated for $H = 0.225 \mu\text{m}$, $h = 0.215 \mu\text{m}$, $w = 2.0 \mu\text{m}$ and for two values of the cover refractive index: $n_c = 1.00$ and 1.33 .

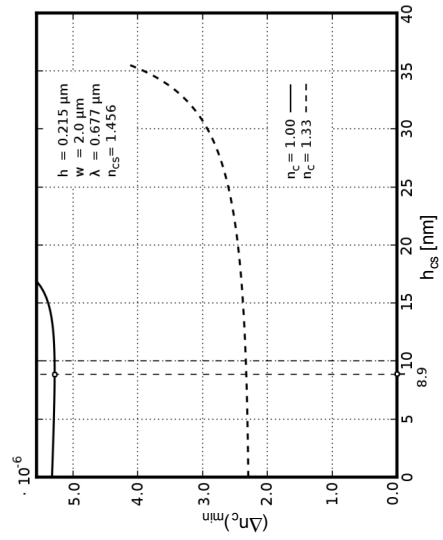
waveguides characterized by $h = 0.215 \mu\text{m}$ and $w = 2.0 \mu\text{m}$. Two pairs of these characteristics are shown in Fig. 11. The first pair is calculated for $n_c = 1.00$. It can be seen that a decrease in the detection limit is considerable for wavelengths higher than $\lambda \approx 700 \text{ nm}$. The wavelength at which the $(\Delta n_c)_{\min}$ is minimal is higher for the rib waveguide. The second pair is calculated for $n_c = 1.33$. The differences observed for the parent slab and the rib waveguide can be neglected.

The imperfections of rib waveguide sidewalls cause the scattering-induced attenuation. This attenuation depends on the difference between a rib refractive index n_r and a cover refractive index n_c . Sol-gel technology also allows silica layers to be fabricated [22, 23]. Such a layer can separate the sidewalls from ambient and decrease a refractive index contrast on the sidewalls. The influence for a thickness h_{cs} of such a layer on the effective refractive index and homogeneous sensitivity characteristics of the rib waveguide is shown in Fig. 12. The increase of h_{cs} results in an increase of the effective index values and decrease of the homogeneous sensitivity values. The dashed vertical line at $h_{cs} = 10 \text{ nm}$ is related to condition $h_{cs} = t$. The relative decrease in homogeneous sensitivity related to the presence of an additional layer is higher for TE_{00} mode and increases with an increase in n_c . For TE_{00} mode, $n_c = 1.33$ and $h_{cs} = 10 \text{ nm}$ the relative decrease in sensitivity is relatively small: $\delta_{SH} \approx 3.3\%$.

Under the same conditions the characteristics of estimated detection limits for Δn_c as a function of h_{cs} were calculated for the rib waveguides characterized by $d = 0.215 \mu\text{m}$, $w = 2 \mu\text{m}$. These characteristics for $n_c = 1.00$ and 1.33 are shown in



▲ Fig. 12. The effective index n_{eff} characteristics (a) and homogeneous sensitivity S_H characteristics (b) as a function of a thickness h_{cs} of a separating silica layer calculated for the rib waveguide whose morphological parameters are presented in Fig. 1c. Characteristics calculated for $H = 0.225 \mu\text{m}$, $h = 0.215 \mu\text{m}$, $w = 2.0 \mu\text{m}$, $n_{\text{cs}} = 1.456$, $\lambda = 0.677 \mu\text{m}$ and for two values of the cover refractive index: $n_c = 1.00$ and 1.33 .



▼ Fig. 13. The cover refractive index detection limit $(\Delta n_c)_{\text{min}}$ characteristics as a function of a thickness h_{cs} of a separating silica layer calculated for a rib waveguide whose morphological parameters are presented in Fig. 1c. Characteristics calculated for $H = 0.225 \mu\text{m}$, $h = 0.215 \mu\text{m}$, $w = 2.0 \mu\text{m}$, $n_{\text{cs}} = 1.456$, $\lambda = 0.677 \mu\text{m}$ and for two values of the cover refractive index: $n_c = 1.00$ and 1.33 .

Fig. 13. Their profile is governed by the difference in homogeneous sensitivity characteristics of TE₀₀ and TM₀₀ modes. For $n_c = 1.00$ the characteristic has the minimum at $h_{cs} \approx 9.0$ nm, whereas for $n_c = 1.33$ the value of $(\Delta n_c)_{\min}$ is monotonically increasing and the relative increase in $(\Delta n_c)_{\min}$ for a separating layer of thickness $h_{cs} = 10$ nm is $\delta_{cs} \approx 1.7\%$.

6. Conclusions

This work presents a theoretical analysis of the relation between the geometrical parameters of the sol–gel derived SiO₂:TiO₂ single modal rib waveguides and their homogeneous sensitivity. The analysis was performed using the effective index method. Because the analysis was carried out in view of the rib waveguides fabricated by means of selective etching of the slab waveguide, the modal and homogeneous sensitivity characteristics of the rib waveguides are compared with the ones of the parent slab waveguide.

The spectral range in which rib waveguides are single modal depends strongly on etching depth t . The calculations showed that the rib waveguides are single modal for small etching depths. It was shown that formation of a rib decreases or increases the values of the homogeneous sensitivity. For a given rib waveguide and its parent slab, for a given polarization and cover refractive index there exists one wavelength λ^* for which the values of their homogeneous sensitivities are equal. For shorter wavelengths the sensitivity of the rib waveguide is higher comparing to the parent slab waveguide, whereas for longer wavelengths is lower. The magnitude of sensitivity decrease is dependent on how much the wavelength is outlying from the λ^* and on a value of the cover refractive index n_c . This magnitude is decreasing along with an increase in n_c . For rib waveguides based on the parent slab described, for $n_c = 1.33$ and $\lambda = 677$ nm the changes are very small. This is mirrored on the spectral characteristic of the cover refractive index detection limit. Considerable changes in $(\Delta n_c)_{\min}$ are present for $n_c = 1.00$ and $\lambda > 700$ nm. For $n_c = 1.33$ the changes are negligible in a full span of the spectral range presented. Moreover, it was shown that the presence of the silica layer separating the rib sidewalls from ambient slightly decreases the sensitivity. The magnitude of this change is increasing along with an increase in cover refractive index, thickness of separating film and is also polarization dependent – it is higher for TE₀₀ mode. It was shown that for completely separated sidewalls, $h_{cs} = 10$ nm, a relative decrease of S_H for $n_c = 1.33$, $\lambda = 677$ nm and TE₀₀ mode is $\delta_{SH} \approx 3.3\%$. The corresponding relative increase in the cover refractive index detection limit is $\delta_{cs} \approx 1.7\%$.

Acknowledgements – This work was sponsored by the Polish National Science Center under the Grant DEC-2011/01/B/ST7/06525.

References

- [1] RICHARDSON K., PETIT L., CARLIE N., ZDYRKO B., LUZINOV I., HU J., AGARWAL A., KIMERLING L., ANDERSON T., RICHARDSON M., *Progress on the fabrication of on-chip, integrated chalcogenide glass (CHG)-based sensors*, Journal of Nonlinear Optical Physics and Materials **19**(1), 2010, pp. 75–79.
- [2] KEE. J.S., POENAR D.P., NEUZIL P., YOBAS L., *Design and fabrication of poly(dimethylsiloxane) single-mode rib waveguide*, Optics Express **17**(14), 2009, pp. 11739–11746.
- [3] POENAR D.P., KEE J.S., NEUZIL P., YOBAS L., *The design and fabrication of poly(dimethylsiloxane) single mode rib waveguides for lab-on-a-chip applications*, Advanced Materials Research **74**, 2009, pp. 51–54.
- [4] ROGOZIŃSKI R., KARASIŃSKI P., *Optical waveguides produced in ion exchange process from the solutions of $\text{AgNO}_3\text{--NaNO}_3$ for planar chemical amplitude sensors*, Opto-Electronics Review **13**(3), 2005, pp. 229–238.
- [5] CHAKRABORTY R., GANGULY P., BISWAS J.C., LAHIRI S.K., *Modal profiles in Ti:LiNbO_3 two-waveguide and three-waveguide couplers by effective-index-based matrix method*, Optics Communications **187**(1–3), 2001, pp. 155–163.
- [6] KOLLAKOWSKI S., LEMM C., STRITTMATTER A., BOTTCHEER E.H., BIMBERG D., *Buried InAlGaAs–InP waveguides: etching, overgrowth, and characterization*, IEEE Photonics Technology Letters **10**(1), 1998, pp. 114–116.
- [7] FERGUSON A.D., KUVER A., HEATON J.M., ZHOU Y., SNOWDEN C.M., IEZEKIEL S., *Low-loss, single-mode GaAs/AlGaAs waveguides with large core thickness*, IEE Proceedings Optoelectronics **153**(2), 2006, pp. 51–56.
- [8] KARASIŃSKI P., TYSZKIEWICZ C., ROGOZIŃSKI R., JAGLARZ J., MAZUR J., *Optical rib waveguides based on sol–gel derived silica–titania films*, Thin Solid Films **519**(16), 2011, pp. 5544–5551.
- [9] KARASIŃSKI P., TYSZKIEWICZ C., ROGOZIŃSKI R., *Rib waveguides based on the sol–gel derived $\text{SiO}_2:\text{TiO}_2$ films*, Photonics Letters of Poland **2**(1), 2010, pp. 40–42.
- [10] KARASIŃSKI P., TYSZKIEWICZ C., ROGOZIŃSKI R., *Single-mode rib waveguides fabricated by means of sol–gel method*, Acta Physica Polonica A **118**(6), 2010, pp. 1168–1170.
- [11] KARASIŃSKI P., ROGOZIŃSKI R., TYSZKIEWICZ C., *Żebrowe światłowodowy paskowe do zastosowań sensorowych*, Pomiar Automatyka Kontrola, No. 6, 2010, pp. 541–543, (in Polish).
- [12] KARASIŃSKI P., TYSZKIEWICZ C., ROGOZIŃSKI R., *Optical channel structures based on sol–gel derived waveguide films*, Optica Applicata **41**(2), 2011, pp. 351–357.
- [13] KARASIŃSKI P., *Embossable grating couplers for planar evanescent wave sensors*, Opto-Electronics Review **19**(1), 2011, pp. 10–21.
- [14] TYSZKIEWICZ C., KARASIŃSKI P., ROGOZIŃSKI R., *Sol–gel derived sensitive films for ammonia sensors*, Acta Physica Polonica A **118**(6) 2010, pp. 1262–1266.
- [15] KARASIŃSKI P., *Sensor properties of planar waveguide structures with grating couplers*, Opto-Electronics Review **15**(3), 2007, pp. 168–178.
- [16] KARASIŃSKI P., *Optical uniform/gradient waveguide sensor structure – characterization*, Opto-Electronics Review **19**(1), 2011, pp. 1–9.
- [17] BOISDE G., HARMER A., *Chemical and Biochemical Sensing with Optical Fibres and Waveguides*, Artech House, Boston–London, 1996.
- [18] LUKOSZ W., *Integrated optical chemical and direct biochemical sensors*, Sensors and Actuators B **29**(1–3), 1995, pp. 37–50.
- [19] PARRIAUX O., VELDHIJS G.J., *Normalized analysis for the sensitivity optimization of integrated optical evanescent-wave sensors*, Journal of Lightwave Technology **16**(4), 1998, pp. 573–582.
- [20] LACEY J.P.R., PAYNE F.P., *Radiation loss from planar waveguides with random wall imperfections*, IEE Proceedings J Optoelectronics **137**(4), 1990, pp. 282–288.

- [21] KIN SENG CHIANG, *Effective-index analysis of optical waveguides*, Proceedings of SPIE **2399**, 1995, pp. 2–12.
- [22] KARASIŃSKI P., JAGLARZ J., REBEN M., SKOCZEK E., MAZUR J., *Porous silica xerogel films as antireflective coatings – Fabrication and characterization*, Optical Materials **33**(12), 2011, pp. 1989–1994.
- [23] JAGLARZ J., KARASIŃSKI P., SKOCZEK E., *Optical properties of silica antireflective films formed in sol–gel processes*, Physica Status Solidi (C) **8**(9), 2011, pp. 2645–2648.

*Received July 27, 2011
in revised form February 18, 2012*